Available online at www.sciencedirect.com
SCIENCE DIRECT®
Journal of Organometallic Chemistry 690 (2005) 5150–5158
Journal of Organometallic Chemistry
www.elsevier.com/locate/jorganchem

The role of phosphine in cobalt-catalyzed carbonylative polymerization of *N*-alkylaziridine

Hongyu Xu [a], Nathalie LeGall [a], Li Jia [a,*], William W. Brennessel [b], Benjamin E. Kucera [b]

[a] *Department of Chemistry, Lehigh University, 6 E. Packer Avenue, Bethlehem, PA 18015, USA*
[b] *Department of Chemistry, University of Minnesota, Minneapolis, MN 55455, USA*

Received 15 February 2005; received in revised form 25 March 2005; accepted 28 March 2005
Available online 23 May 2005

Abstract

A series of $CH_3COCo(CO)_3L$ complexes (**1**, L = PCy_3; **2**, L = PMe_2Ph; **3**, L = PPh_3; 4, L = P(*para*-F-Ph)$_3$; **5**, L = P(*meta*-F-Ph)$_3$; and **6**, L = P(*ortho*-tolyl)$_3$) were studied as precatalyst for the title polymerization. The Co–P bond length primarily responds to the cone angle of the phosphine ligand (**6** > **1** > **2** ≈ **3** ≈ **4** ≈ **5**), while the back-donation to the axial acetyl ligand and the equatorial CO ligand depends on the electron-donating ability of the phosphine and increases in the order **1** > **6** > **2** > **3** > **4** > **5**. The equilibrium constant for $CH_3COCo(CO)_3L + CO \leftrightarrow CH_3COCo(CO)_4 + L$ depends on the electron-donating ability of the phosphine ligand except for **6** and follows the order **6** ≫ **5** > **4** > **3** > **2** > **1**. The catalytic activity follows the order **6** > **5** > **4** > **3** > **1** > **2**. The activity difference cannot be explained solely by the above equilibrium and is consistent with the competition for the acyl site by the phosphine as nucleophile against aziridine. The production of the β-lactam byproduct is attributed to catalyst decomposition, which is accelerated to the basicity/nucleophilicity of the phosphine ligand.

Keywords: Catalysis; Carbonylative polymerization; Polyamide

1. Introduction

Metal-catalyzed carbonylation has been used in the synthesis of a broad spectrum of organic carbonyl compounds [1–7]. However, the use of carbonylation in polymer synthesis has primarily been focused on polyketone synthesis [8–17]. A few early reports and patents in the 1960s disclosed that inorganic compounds of group 8–10 metals, some times in the presence of main group organometallic compounds, catalyzed copolymerizations of CO and oxygen containing comonomers [18–23]. Radical initiated CO–aziridine copolymerization was also reported in 1966 [24]. Unfortunately, these reports attracted little attention or further research activity perhaps owing to the overwhelming focus on condensation polymerizations at the time. In view of the current demand for functional and environmentally benign polymeric materials [25–27], the idea of obtaining polyesters and polyamides through direct carbonylative polymerization of heteroatom-containing monomers (COPH) deserves reassessment. Particularly, the carbonylative approach should serve as an alternative method for the synthesis of these advanced materials complementary to the relatively established methods of ring-opening polymerization of lactones and lactams [28–34]. In 1997, Sen [35,36] reported an oxidative carbonylative polymerization producing polysuccinates. Further, in 1998, Sen and Arndtsen independently proposed the CO–imine copolymerization as a way of synthesizing polypeptides [37–39]. Although the copolymerization proposed by Sen and Arndtsen has yet to be realized, they demonstrated the first example of stoichiometric

* Corresponding author. Tel.: +1 6107585715; fax: +1 6107586536.
E-mail address: lij4@lehigh.edu (L. Jia).

0022-328X/$ - see front matter © 2005 Elsevier B.V. All rights reserved.
doi:10.1016/j.jorganchem.2005.03.050

imine insertion into metal–acyl bonds, a necessary reaction for the copolymerization to occur. Several groups have noted that the $Co_2(CO)_8$/3-hydroxypyridine catalyst system produces polyester as the major product in contrary to the patent report that β-lactones were the major products [7] and have subsequently studied the binary catalyst systems based on $Co_2(CO)_8$ [40–45]. We have been interested in the design and development of carbonylative polymerization of COPH using the de novo approach based on well-defined single-site molecular catalysts. We reported in 2001 the first example of metal-catalyzed carbonylative polymerization of aziridine under the hypothesis that aziridine enchainment would occur via sequential nucleophilic reactions as shown in Scheme 1 [46]. In the past several years, we investigated the hetero-atom-containing substrates including *N*-alkylaziridnes, 2-oxazolines, epoxides, *N*-alkylazetidines, and THF [47–52]. Darensbourg's group directly investigated the kinetics and mechanism of the *N*-alkylaziridine carbonylative polymerization in a joint effort with us [53]. The study substantiated the mechanism that we proposed for the polymerization and yielded an important proposition that the phosphine ligand suppresses the polymerization rate by competing against the aziridine monomer for the acyl-site as shown in Scheme 2. Further, a back-biting depolymerization mechanism was proposed for the formation of β-lactam byproduct when the PPh_3 ligand is present in the polymerization system.

The goal of this work is to investigate further the effect of the phosphine on the polymerization rate and the formation of the β-lactam byproduct. A series of complexes bearing phosphine with varied electronic and steric characteristics was synthesized and studied as precatalysts for the carbonylative polymerization of *N*-butylaziridine. While all evidences support the mechanism in Scheme 2 for the suppression of the polymerization rate, we propose here an alternative explanation for the formation of β-lactam byproduct.

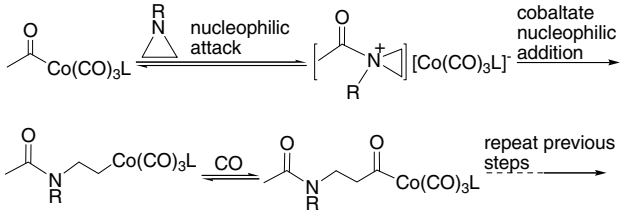

Scheme 1. Mechanism for carbonylative polymerization of aziridines.

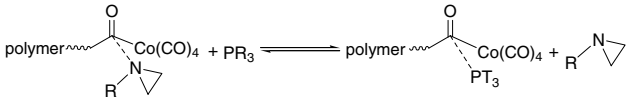

Scheme 2. Competition between phosphine and aziridne for the acyl site.

2. Experimental

All manipulations were performed in a Vacuum Atmosphere DRI-LAB-08/85 dry box under a nitrogen atmosphere or using standard Schlenk line techniques. Diethyl ether, *n*-hexane and tetrahydrofuran (THF) were dried by refluxing over sodium/benzophenone under nitrogen. Toluene was dried by refluxing over sodium under nitrogen. Benzene-d_6 was dried over Na/K alloy, freeze–pump–thaw degassed, and kept over Na/K alloy. $NaCo(CO)_4$ was synthesized according to the published procedure [54]. *N*-butylaziridine was synthesized using a modified method from literature [55], dried by Na/K alloy, and kept over Na/K alloy. The purity of the monomers is crucial for maximizing the catalyst turnover number. The complex $CH_3C(O)Co(CO)_3(PPh_3)$ were prepared by a modified literature procedures [56].

The ^1H NMR spectra were recorded with an AMX 360 MHz or a DRX 500 MHz NMR spectrometer. The ^1H and ^{13}C chemical shifts were measured using the solvent resonances as internal references. The ^1H and ^{13}C NMR spectra of the polymer in d_2-1,1, 2,2-tetrachloroethane are consistent with its proposed structure. GC/MS were obtained with a Hewlett–Packard 5890 series instrument. The elemental analyses were performed by Micro-analysis Inc., DE. Infrared spectra were recorded on an ASI ReactIR 4000 system equipped with a MCT detector. The resolution of all collected data was set to be 4 cm^{-1}.

GPC analyses of the molecular weight of the polymer products were performed using chloroform as the solvent, with a Waters 1515 isocratic HPLC pump and Waters 2414 refractive index detectors at 35 °C. The column set was composed of one styragel HR 5E column and two HR2 columns, targeting the molecular weight region from 1000 to 10,000 but also covering molecular weight up to 100,000.

2.1. Synthesis of $CH_3C(O)Co(CO)_3PCy_3$ (1)

$NaCo(CO)_4$ (0.97 g, 5 mmol) and equimolar tricyclohexylphosphine were loaded into a 100 mL flask in the glove box. The flask was connected to the Schlenk line, evacuated and back-filled with an atmosphere of CO. All the operations were then carried out under a CO atmosphere. Diethyl ether (40 mL) was added to the flask at 0 °C, under stirring to ensure the dissolution of both reactants. After 5 min, an equimolar amount of iodomethane (5 mmol; 0.32 mL) was added via a syringe. After the mixture was stirred at 0 °C for 1 h and at room temperature for 4 additional hours, the solvent

was removed in vacuum at room temperature. The residue was extracted with toluene (2×20 mL), and 40 mL of *n*-hexane was added to induce crystallization of the product. Isolated yield: 1.61 g (70%). Suitable single-crystals for X-ray crystallography studies were obtained from the solution of 1:1 mixture of toluene and *n*-hexane at −30 °C. Anal. Calc. for $C_{23}H_{36}CoO_4P$: C, 59.23; H, 7.78. Found: C, 59.02; H, 7.68. ^{1}H NMR (20 °C, C_6D_6): δ 0.97–1.88 (m, 33H, P(C_6H_{11})$_3$), 2.77 (s, 3H, C(O)CH_3), IR (20 °C, THF, cm^{-1}): υ CO 2038 (w), 1968 (s), 1945 (s); υ C(O)Me, 1675 (m).

2.2. Synthesis of $CH_3C(O)Co(CO)_3PMe_2Ph$ (2)

Complex **2** was synthesized following a procedure similar to that used for **1** except that dimethylphenylphosphine was used as the starting material. The product was extracted with 40 mL of hexane. The hexane solution was stored at −30 °C for a week to give rise to yellow crystals. Isolated yield: 0.83 g (50%). Suitable single-crystals for X-ray crystallography studies were obtained from the *n*-hexane solution at −30 °C. Anal. Calc. for $C_{13}H_{14}CoO_4P$: C, 48.17; H, 4.35. Found: C, 47.90; H, 4.39. ^{1}H NMR (25 °C, C_6D_6): δ −1.00 (d, J = 8.6 Hz, 6H, P(CH_3)$_2$Ph), 2.62 (s, 3H, C(O)CH_3), 6.95–6.97 (m, 3H, C_6H_5), 7.17–7.20 (m, 2H, C_6H_5). IR (25 °C, THF, cm^{-1}): υ CO 2046 (w), 1976 (s), 1957 (s); υ C(O)Me 1678.

2.3. Synthesis of $CH_3C(O)Co(CO)_3P(p\text{-}C_6H_4F)$ (4)

Complex **4** was synthesized following a procedure similar to that used for **1** except that tris(*p*-fluorophenyl) phosphine was used as the starting material. The product was extracted with diethyl ether (2×20 mL) and 20 mL of *n*-hexane was added to induce crystallization of the product. Isolated yield: 1.50 g (61%). Suitable single-crystals for X-ray crystallographic studies were obtained from the hexane solution at −30 °C. Anal. Calc. for $C_{23}H_{15}CoF_3O_4P$: C, 55.00; H, 3.01. Found: C, 54.70; H, 3.13. 1H NMR (20 °C, C_6D_6): δ −2.68 (s, 3H, C(O)CH_3), 6.60 (t, J = 8.5 Hz, 2H, *p*-C_6H_4F)3, 7.15 (t, J = 8.5 Hz 2H, *p*-C_6H_4F). IR (20 °C, THF, cm^{-1}): υ CO 2050 (w), 1980 (s), 1962 (s). υ C(O)Me 1684 (m).

2.4. Synthesis of $CH_3C(O)Co(CO)_3P(m\text{-}C_6H_4F)$ (5)

Complex **5** was synthesized following a procedure similar to that used for **1** except that tri(*m*-fluorophenyl) phosphine was used as the starting material. The residue was extracted with toluene (2×20 mL) and 20 mL of *n*-hexane was added to induce crystallization of the product. Isolated yield: 1.55 g (63%). Suitable single-crystals for X-ray crystallographic studies were obtained from the hexane solution at −30 °C. Anal. Calc. for $C_{23}H_{15}CoF_3O_4P$: C, 55.00; H, 3.01. Found: C, 54.72; H, 3.13. ^{1}H NMR (20 °C, C_6D_6): δ −2.55 (s, 3H, C(O)CH_3), 6.55–6.57 (m, 1H, *m*-C_6H_4F)3, 6.66–6.68 (m, 1H, *m*-C_6H_4F), 7.06–7.08 (m, 1H, *m*-C_6H_4F), 7.16–7.17 (m, 1H, *m*-C_6H_4F). IR (25 °C, THF, cm^{-1}): υ CO 2052 (w), 1984 (s), 1964 (s); υ C(O)Me 1686 (m).

2.5. X-ray structure determination

Crystals of **1**, **2**, **4**, and **5** were placed on the tip of a 0.1 mm diameter glass capillary and mounted on a Siemens or Bruker SMART Platform CCD diffractometer for data collection at 173(2) K. A preliminary set of cell constants was calculated from reflections harvested from three sets of 20 frames. These initial sets of frames were oriented such that orthogonal wedges of reciprocal space were surveyed. The data collection was carried out using Mo Kα radiation (graphite monochromator). A randomly oriented region of reciprocal space was surveyed to the extent of one sphere and to a resolution of 0.77 Å. Four major sections of frames were collected with 0.30° steps in ω at four different φ settings and a detector position of −28° in 2θ. The intensity data were corrected for absorption, and decay (SADABS) [57]. Final cell constants were calculated from the *xyz* centroids of 3421, 2750, 1673, and 2684 strong reflections, respectively, from the actual data collection after integration (SAINT) [58].

The structures were solved by direct methods using SIR2002 [59] for **4** and using SHELXS-97 [60] for **1** and **2** and **5**. The space groups were determined based on systematic absences and intensity statistics. A direct-methods solution was calculated which provided most non-hydrogen atoms from the E-map. Full-matrix least squares/difference Fourier cycles were performed which located the remaining non-hydrogen atoms. All non-hydrogen atoms were refined with anisotropic displacement parameters. All hydrogen atoms were placed in ideal positions and refined as riding atoms with relative isotropic displacement parameters.

For complex **5**, one fluorine is disordered on a –C_6H_4F group in a 0.776:0.224 ratio. The acetyl group is disordered in a 0.646 : 0.354 ratio over two positions rotated by 88°. Restraints were required to force the disordered acetyl groups to be planar with the Co atom, respectively. It was also necessary to tie the anisotropic displacement parameters of C4′ to O4′, since this gave a cigar shaped ellipsoid.

Carystallographic data for the structural analysis have been deposited with the Cambridge Crystallographic Data Center, CCDC No. 266914 for **4**, 266915 for **1**, 266916 for **5**, and 266917 for **3**. Copies of this information may be obtained free of charge from The Director, CCDC, 12 Union Road, Cambridge, CB2 1EZ UK (fax: 44(1223)336-033; or e-mail:

deposit@ccdc.cam.ac.uk or www: http://www.ccdc.cam.ac.uk).

2.6. Polymerization procedure

A 125 mL or 300 mL Parr bomb reactor was evacuated on a Schlenk line and backfilled with CO (1 atm). The aziridine, the catalyst solution, and additional solvent were introduced into the autoclave with syringes under a gentle flow of CO. The reactor was immediately closed, and the pressure of CO was raised to 1000 psi. The reactor was heated in a 60 °C oil bath while being magnetically stirred. After a certain reaction time specified in Table 5, the reactor was allowed to cool to the ambient temperature. The CO pressure was slowly released in a fume hood. The reactor was opened. The solution was transferred into a flask. The crude product was obtained after removal of solvent. Diethyl ether (50 mL) was used to wash away free phosphine and lactam, if any was formed, from the crude product.

2.7. Polymerization monitored by IR spectroscopy

The reactor is modified with a 30 bounce SiCOMP window to allow the use of an ASI ReactIR 4000 system equipped with a MCT detector. In this manner, a single 256-scan background spectrum was collected. The infrared spectrometer was set to collect one spectrum every 2 min over a period up to 48 hours. In a typical experiment, 80 mL of distilled THF was delivered via the injection port into a 300-mL stainless steel Autoclave Engineers autoclave reactor kept under dynamic vacuum overnight at room temperature. After 10 spectra of THF solvent were collected, in the intervals between 10th and 11th spectra, a solution of the cobalt catalyst (15 mmol in 4 mL THF) was injected into the reactor. Between the interval of the 14th and 15th spectra, the reactor was pressurized to 1000 psi and the temperature was raised to 60 °C. After about 2 h under these conditions, the monomer was added through an addition tube at higher pressure. The polymer growth is depicted by the absorbance profile of the amide carbonyl observed at 1644 cm^{-1}.

3. Results and discussion

3.1. Synthesis and characterization of catalysts

Synthesis of compounds **1**, **2**, **4**, and **5** ($CH_3C(O)Co(CO)_3L$: **1**, L = PCy_3; **2**, L = PMe_2Ph; **4**, L = P(*p*-F-Ph)$_3$; **5**, L = P(*m*-F-Ph)$_3$) was straightforward, following modified procedures similar to the one for $CH_3C(O)Co(CO)_3(PPh_3)$ (**3**) reported by Heck [56]. All compounds were purified by recrystallization using appropriate solvents as specified in the Experimental Section. Crystallization of **2** usually requires keeping the orange oil that precipitates out easily upon cooling at −30 °C for a prolonged period. The preparation procedure for **6** was previously reported [53].

The crystal structures of **1**, **2**, **4**, and **5** were determined by X-ray diffraction as shown in Fig. 1. Like the previously reported structures of **3** and **6**, all structures adopt the trigonal bipyramidal conformation, with the CO ligands occupying the equatorial sites and the phosphine and acetyl ligands occupying the axial sites. The bond distances and angles in the coordination core are summarized in Table 1. The acetyl group in **5** is disordered in a 0.646:0.354 ratio over two positions, and only the bond distances in the more abundant component are included in Table 1. One of the fluorophenyl groups in **5** is also disordered over two positions. Only the major occupancies of the acetyl and the fluorophenyl is shown in Fig. 1(d). In the series **1**–**6**, the Co–P distance (2.250(4) and 2.3139(6) Å in **3** and **6**, respectively) apparently changes in response to the cone angle of the phosphine ligand [61]. All other bond distances and bond angles are rather insensitive to the variation of the electronic and steric properties of the phosphine ligand.

The solution IR data are much more informative and perhaps more relevant than the X-ray data. The wave numbers of the stretching vibration of the carbonyl ligands and the C=O bond in the acetyl ligand are summarized in Table 2 with the phosphine-free $CH_3Co(CO)_4$ (**7**) also included. The electron-donating ability of the axial phosphine ligand in the trigonal bipyramidal complexes clearly exerts a consistent effect on both the stretching vibration of the equatorial CO and the stretching vibration of the C=O bond of the acetyl ligand. The latter event has important bearings to the carbonylative polymerization because an increase of back-donation from the Co d_{xz} and d_{yz} orbitals to the π* orbital of the acetyl C=O double bond not only weakens the C=O bond, but also strengths the acetyl-Co bond and thus retards its reactivity toward nucleophiles [62].

3.2. The effect of phosphine on the polymerization

With the series **1**–**6**, we are now able to study systematically the phosphine effect on the polymerization using in situ ATR-IR as the monitoring tool. All of the experiments for elucidating the phosphine effect were carried out under a set of uniform conditions (60 °C, 1000 psi CO, in THF). The first step that we took before performing the polymerization was to determine the equilibrium position between **1**–**6** and the phosphine free **7** at the polymerization temperature and pressure (Eq. (1)). The processes involving the establishment

$$CH_3C(O)Co(CO)_3L + CO \rightleftharpoons CH_3C(O)Co(CO)_4 + L \quad (1)$$

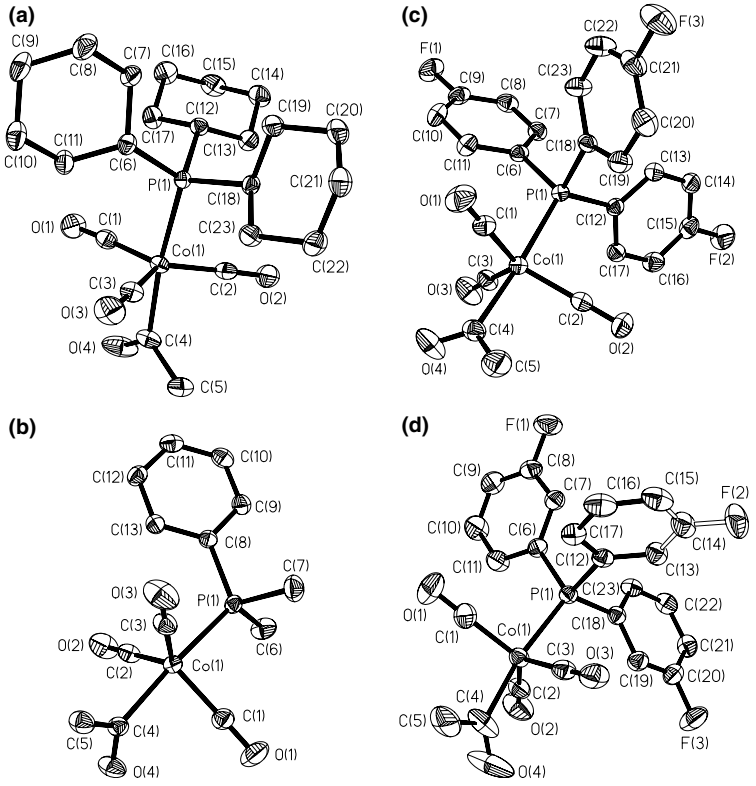

Fig. 1. ORTEP drawings with thermal ellipsoids at 50% probability. Hydrogen atoms are omitted. (a) **1**, (b) **2**, (c) **4**, and (d) **5**.

Table 1
Selected bond lengths and bond angles in **1**, **2**, **4**, and **5**

	1	**2**	**4**	**5**
Bond length (Å)				
Co(1)–C(1)	1.8029(14)	1.7809(17)	1.771(2)	1.786(2)
Co(1)–C(2)	1.7740(14)	1.7757(19)	1.791(2)	1.789(2)
Co(1)–C(3)	1.7777(13)	1.7879(18)	1.792(2)	1.779(2)
Co(1)–C(4)	2.0105(13)	2.0133(16)	2.007(2)	2.019(3)
Co(1)–P(1)	2.2776(3)	2.2414(5)	2.2485(6)	2.2472(5)
C(4)–O(4)	1.1949(18)	1.204(2)	1.199(3)	1.212(5)
Bond angle (°)				
C(1)–Co(1)–C(2)	120.89(6)	119.97(8)	120.91(10)	116.08(10)
C(1)–Co(1)–C(3)	110.89(6)	118.71(8)	122.71(10)	117.43(10)
C(2)–Co(1)–C(3)	127.49(6)	121.09(8)	115.44(10)	125.93(10)
C(4)–Co(1)–P(1)	173.06(4)	174.83(5)	175.55(6)	170.83(10)
O(4)–C(4)–Co(1)	123.44(11)	122.06(12)	122.04(17)	120.6(3)

Table 2
IR data (hexane, RT) of the $CH_3Co(CO)_3PR_3$ complexes

$CH_3C(O)Co(CO)_3L$	L	$\nu_{C\equiv O}$ (cm^{-1})	$\nu_{(C=O)Me}$ (cm^{-1})
1	PCy_3	2041(w), 1970(s), 1949(s)	1685(m)
2	PMe_2Ph	2048(w), 1979(s), 1961(s)	1689(m)
3	PPh_3	2051(w), 1983(s), 1963(s)	1691(m)
4	P(*p*-C_6H_4F)	2052(w), 1985(s), 1965(s)	1692(m)
5	P(*m*-C_6H_4F)	2054(w), 1987(s), 1969(s)	1698(m)
6	P(*o*-Tol)	2047(w), 1980(s), 1959(s)	1686(m)
7	CO	2107(w), 2025(s), 2010(s)	1722(m)

of the equilibrium and the subsequent polymerization were monitored by in situ ATR IR. Upon subjecting **6** to the above specified temperature and pressure, complete conversion to **7** was observed instantaneously. For **1**–**5**, the IR band of the lowest wave number CO stretching vibration in each case is completely or nearly completely separated from the IR absorptions of **7** (Table 2). Monitoring the decrease of the lowest-frequency CO absorbance over time allows the observation of the equilibrium, which takes about 10–15 min to establish. Two examples of the in situ IR plots are shown in Figs. 2 and 3. Under the reasonable assumption that the conversion to **7** accounts for the entire loss of **1**–**6**, the equilibrium constants and concentrations of **7** at equilibrium can be obtained (Table 3). With the exception of **6**, the phosphine electron-donating ability apparently governs the equilibrium position. The equilibrium position does not follow the same trend as the Co–P bond distance in the solid state.

After the equilibrium was established, *N*-butylaziridine was injected into the autoclave under high pressure via a slightly overpressurized addition tube (Figs. 2 and 3). Polymerization immediately started as evidenced by the growth of the absorbance at 1644 cm^{-1}. A new IR band at 1890 cm^{-1} attributable to $Co(CO)_4^-$ also appeared immediately after the reaction was started in all cases with **1**–**6** as the precatalyst. The lowest frequency CO absorption from acyl-$C(O)Co(CO)_3L$ does not noticeably shift during the entire reaction, but its absorbance dwindles somewhat as the polymerization proceeds. Assuming that the molar absorbability is not affected by the chain growth, the above observation

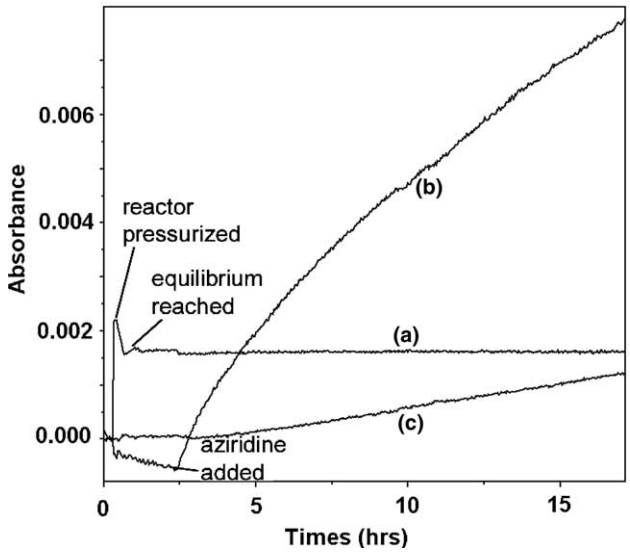

Fig. 2. (a) Change of the concentration of **2** depicted by the absorbance profile at 1957 cm^{-1}. (b) Polymer growth depicted by the absorbance profile of the amide carbonyl at 1644 cm^{-1}. (c) Lactam formation depicted by the absorbance profile of the amide carbonyl at 1750 cm^{-1}.

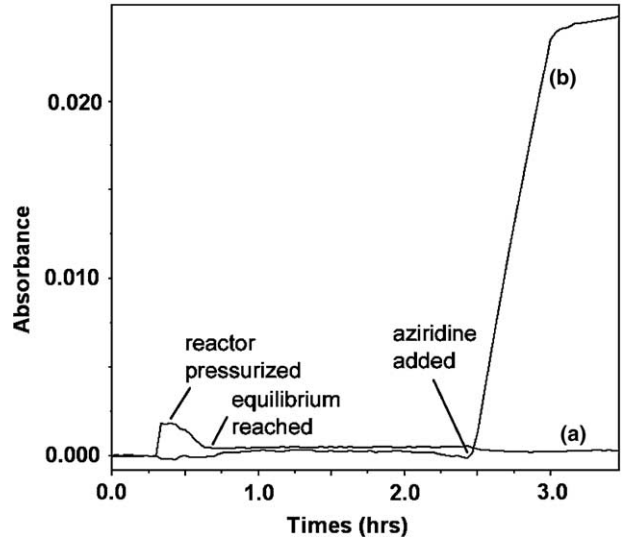

Fig. 3. (a) Change of the concentration of **5** depicted by the absorbance profile at 1964 cm^{-1}. (b) Polymer growth depicted by the absorbance profile of the amide carbonyl at 1644 cm^{-1}.

Table 3
Equilibria between **1**–**6** and **7** at 60 °C under 1000 psi CO in THF

$CH_3C(O)Co(CO)_3PR_3$		Conversion to **7** (%)	K ($M\ bar^{-1}$)
PCy_3	**1**	13	4.8×10^{-7}
PMe_2Ph	**2**	29	2.9×10^{-6}
PPh_3	**3**	46	9.7×10^{-6}
P(*p*-C_6H_4F)	**4**	67	3.4×10^{-5}
P(*m*-C_6H_4F)	**5**	82	9.2×10^{-5}
P(*o*-Tol)	**6**	100	Large

indicates that the concentration of acyl-$C(O)Co(CO)_3L$ is the highest at the beginning of the polymerization and decreases somewhat as the polymerization proceeds. A direct comparison of the rate constants was impossible because the order of rate dependence on aziridine concentration appeared to be different when different catalysts were used. Two forms of kinetic profiles for the polymer growth were observed as exemplified by Figs. 2 and 3. For precatalysts **5** and **6**, the polymer growth profile appeared to be independent of the aziridine concentration. For precatalysts **1**–**4**, the rate dependence deviates more and more from the zero-order dependence to a positive-order dependence on aziridine concentration. We therefore opted to use the half-life of reaction and the initial rate for the rate comparison. The half-life and the initial rate of the polymerization are significantly affected by the electronic and steric properties of the various phosphines (Table 4). It is tempting to explain the rate difference based on the equilibrium involving the phosphine-ligated $RC(O)Co(CO)_3L$ species and the phosphine-free $RC(O)Co(CO)_4$ species (Eq. (1)) during the polymerization because it is not unreasonable to anticipate that the former are inactive or much less active than the latter since the electron-donating phosphine ligand inhibits the reactivity of the acyl-Co bond toward nucleophiles (vide supra). According to the concentrations of **7** established by the aforementioned equilibrium study (Table 3), the polymerization rates catalyzed by precatalyst **1**–**6** should display the following ratio: 0.13:0.29:0.46:0.67:0.82:1. In reality, the ratio of the reciprocal of the reaction half-life is 0.039:0.030:0.16:0.31:0.69:1, and the ratio of the observed initial rate is 0.068:0.068:0.20:0.29:0.69:1. Therefore, regardless of how the comparison is made, the partial existence of the catalyst in the presumed inactive form is not enough to completely account for the decrease of reaction rate, particularly in the cases where the basicity of the phosphine ligand is relatively strong. Further contradicting the explanation solely based on the inactivity of acyl-$Co(CO)_3L$ is that **2** is a somewhat slower precatalyst than **1**, but more **7** is at equilibrium with **2** than with **1** under 1000 psi CO. On the other hand, the alternative mechanism that Darensbourg and we proposed for the phosphine effect on the polymerization can be easily applied

Table 4
Comparison of the polymerization rate[a]

Precatalyst	Reaction half-life (min)	Initial rate ($\times10^{-6}$ mol L^{-1} s^{-1})
1	278	4.2
2	366	4.2
3	68	12.2
4	35	17.8
5	16	42.2
6	11	61.4

[a] Each experiment was conduct in 88 mL THF with 15 mmol of precatalyst, 1000 psi of CO pressure, internal temperature of reactor was 60 °C, reaction monitored by ATR-IR.

Table 5
Carbonylative polymerization of *N*-butylaziridine using **1**–**6** as precatalyst

Entry	Catalyst	Aziridine/cat molar ratio	Reaction time (h)	Yield (%)[a]		M_n ($\times 10^3$)[b]	PDI[b]
				Polymer	Lactam		
1[c]	**1**	40	16	92	8	9.72	1.71
2[c]	**2**	40	16	90	10	6.00	1.71
3[c]	**3**	40	12	97	3	9.68	1.54
4[c]	**4**	40	4	98	2	9.30	1.39
5[c]	**5**	40	4	99	1	8.85	1.32
6[c]	**6**	40	4	100	0	10.45	1.15
7[c]	**5**	31	24	100	0	6.89	1.32
8[d]	**5**	46	24	99	1	9.98	1.32
9[d]	**5**	80	24	95	5	17.0	1.38
10[d]	**6**	21	24	100	0	5.53	1.15
11[d]	**6**	27	24	100	0	7.36	1.16
12[d]	**6**	34	24	100	0	8.89	1.13
13[d]	**6**	62	24	100	0	16.0	1.15
14[d]	**6**	72	24	100	0	17.6	1.11
15[d]	**6**	120	24	97	3	30.1	1.40

[a] The total conversion is essentially quantitative for all the experiments. Product ratio estimated by ^{1}H NMR.
[b] Determined by GPC with a refractive index detector using chloroform as eluent relative to polystyrene standards.
[c] Reaction conditions: 15 mmol of complex; 1000 psi of CO pressure; 88 mol of THF; internal temperature at 60 °C, reaction monitored by ATR-IR.
[d] [catalyst] = 1.70 mM, reactions were run in a regular autoclave placed in an oil bath at 60 °C.

to explain the observed rate difference (Scheme 2). Particularly, it is conceivable that PMe_2Ph is a better carbon nucleophile than PCy_3 because of the steric factors, and therefore would suppress the aziridine enchainment more strongly than the latter.

3.3. Catalyst decomposition and lactam byproduct

As summarized in Table 5, the amount of lactam byproduct varied from negligible to 10% when different precatalysts were used. A back-biting, depolymerization mechanism was previously proposed to explain the formation of the β-lactam [53]. Despite the unfavorable enthalpy for the depolymerization, this mechanism remains a possibility if the entropy could compensate for the enthalpy. On the other hand, it appears always likely that catalyst decomposition is responsible for the byproduct formation in any catalytic processes. In fact, the formation of lactam does not immediately occur at the beginning of the polymerization but slightly lags behind (Fig. 2). This induction period for lactam formation is consistent with the progression of catalyst decomposition. Under such a scenario, the lactam production does not involve the prior formation of the polyamide. Also consistent with the explanation involving catalyst decomposition is that the molecular weight distribution is broadened whenever the β-lactam byproduct is produced (Table 5). For precatalysts **5** and **6** where the β-lactam byproduct is absent or minimal, the number average molecular weight increases linearly as the monomer loading is increased (Figs. 4 and 5).

The above observations prompted us to study the catalyst decomposition process. The decomposition of **2** under the typical polymerization conditions in the absence of a monomer is negligible as monitored by the ReactIR over prolonged time. At 120 °C under 1000 psi CO, the decomposition of **2** occurred over a period of 12 hours and afforded a cobaltate species. The decomposed catalyst solution is active for the carbonylation of aziridine and converts 40 equivalents of *N*-butylaziridine to the β-lactam and the polymer in 2:1 ratio. Although we cannot characterize the counter-cation in the decomposed catalyst, we speculate that it is a possibly a Lewis acid in view of Coates' formulation of $[\text{Lewis acid}]^+[Co(CO)_4]^-$ as potent catalysts for the ring-expanding carbonylation of aziridines. Although the decomposition of **2** only occurs at much higher temperature than the polymerization temperature, it is conceivable that upon the carbonylative enchainment of aziridine, the chain end unit would undergo similar decomposition more readily.

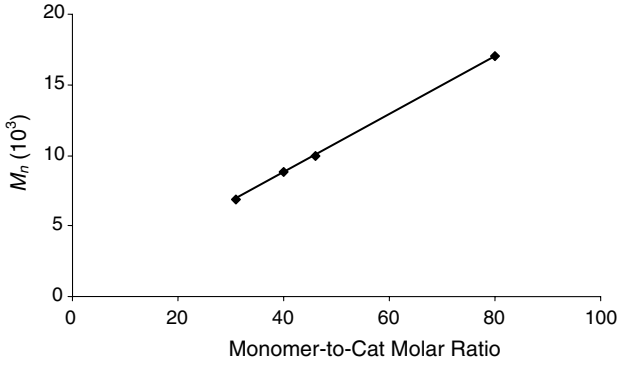

Fig. 4. Linear increase of M_n vs monomer conversion with **5** as the precatalyst.

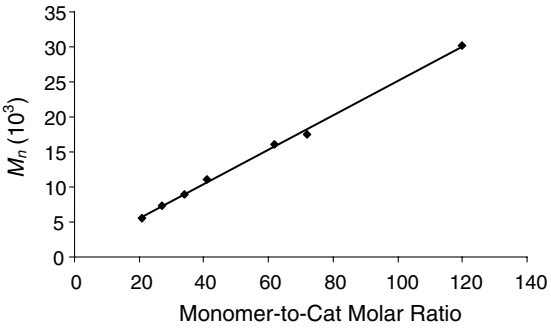

Fig. 5. Linear increase of M_n vs monomer conversion with **6** as the precatalyst.

4. Conclusion

By studying the catalytic behavior of a series of precatalysts for the aziridine carbonylative polymerization, we have shown further evidence that the nucleophilic competition for the acyl site between the phosphine and the monomer is largely responsible for the inhibition of the polymerization in the presence of a phosphine ligand. The coordination of the phosphine ligand to cobalt might also be partially responsible for the rate decrease but is not adequate to explain the large magnitude of the rat decrease. We propose to attribute the formation of β-lactam byproduct to the catalyst decomposition. We have shown that the decomposed catalyst solution is indeed capable of catalyzing the ring-expanding aziridine carbonylation.

Acknowledgments

This work was supported by the Petroleum Research Fund and the National Science Foundation (CAREER). L. J. thanks the DuPont Company for a DuPont Young Professor Award.

Appendix A. Supplementary data

Complete details for the crystallographic study of compounds **1, 2, 4,** and **5**. Supplementary data associated with this article can be found, in the online version at doi:10.1016/j.jorganchem.2005.03.050.

References

[1] K. Khumtaveeporn, H. Alper, Acc. Chem. Res. 28 (1995) 414–422.
[2] P. Davoli, A. Forni, I. Moretti, F. Prati, G. Torre, Tetrahedron 57 (2001) 1801–1812.
[3] P. Davoli, I. Moretti, F. Prati, H. Alper, J. Org. Chem. 64 (1999) 518–521.
[4] W. Chamchaang, A.R. Pinhas, J. Org. Chem. 55 (1990) 2943–2950.
[5] Y.D.Y.L. Getzler, V. Mahadevan, E.B. Lobkovsky, G.W. Coates, J. Am. Chen. Soc. 124 (2002) 1174–1175.
[6] T.L. Lee, P.J. Thomas, H. Alper, J. Org. Chem. 166 (2001) 5424–5426.
[7] E. Drent, E. Kragtwijk, Shell Oil Company, Patent Application: US 5310948, 1994.
[8] C. Bianchini, A. Meli, Coord. Chem. Rev. 225 (2002) 35–66.
[9] E. Drent, P.H.M. Budzelaar, Chem. Rev. 96 (1996) 663–681.
[10] A. Sen, Acc. Chem. Res. 26 (1993) 303–310.
[11] S. Lom, D. Takeuchi, K. Osakada, J. Am. Chem. Soc. 124 (2002) 762–763.
[12] B. Sesto, G. Consiglio, J. Am. Chem. Soc. 123 (2001) 4097–4098.
[13] C.S. Shultz, J. Ledford, J.M. DeSimone, M. Brookhart, J. Am. Chem. Soc. 122 (2000) 6351–6356.
[14] A.L. Safir, B.M. Novak, J. Am. Chem. Soc. 120 (1998) 643–650.
[15] B. Domhover, W. Klaui, A. Kremer-Aach, R. Bell, D. Mootz, Angew. Chem., Int. Ed. 37 (1998) 3050–3052.
[16] A.X. Zhao, J.C.W. Chien, J. Polym. Sci., Part A 30 (1992) 2735–2747.
[17] U. Klabunde, T.H. Tulio, D.C. Roe, S.D. Ittel, J. Organomet. Chem. 334 (1987) 141.
[18] I. Hiroshi, J. Furukawa, T. Mieda, F. Hiroyasu, Bridgestone Tire Co., Ltd, Patent Application: JP 19641103, 1968.
[19] G.L. Bata, K.P. Singh, Union Carbide Canada Ltd., Patent Application: CA 19670818, 1969.
[20] J.F. Nelson, I. Kirshenhbaum, Esso Research and Engineering Co., Patent Application: US 19640626, 1968.
[21] S. Sugiura, T. Ishii, N. Takigawa, Ube Industries, Ltd., Patent Application: JP 19641218, 1968.
[22] M. Modena, M. Ragazzini, E. Gallinella, Polym. Lett. 1 (1963) 567–570.
[23] J. Furukawa, H. Iseda, T. Saegusa, H. Fujii, Makromol. Chem. 89 (1965) 263–268.
[24] T. Kagiya, S. Narisawa, T. Ichida, K. Fukui, H. Yokota, J. Polym. Sci., Part A-1 4 (1966) 293–299.
[25] R.P. Cheng, S.H. Gellman, W.F. DeGrado, Chem. Rev. 101 (2001) 3219–3232.
[26] D. Seebach, J.L. Matthews, Chem. Commun. (1997) 2015–2022.
[27] T.J. Deming, Adv. Drug Delivery Rev. 54 (2002) 1145–1155.
[28] A.-C. Albertsson, I.K. Varma, Biomacromolecules 4 (2003) 1466–1486.
[29] J. Cheng, T.J. Deming, J. Am. Chem. Soc. 123 (2001) 9457–9458, and references therein.
[30] H. Kricheldorf, α-Aminoacid-*N*-carboxyanhydrides and Related Heterocycles, Springer, New York, 1987.
[31] K. Hashimoto, J. Yasuda, M. Kobayashi, J. Polym. Sci., Part A 37 (1999) 909–915, and references therein.
[32] A.M. Ilarduya, C. Alaman, M. Garcia-Alvarez, F. López-Carrasquero, S. Muñoz-Guerra, Macromolecules 32 (1999) 3257–3263, and references therein.
[33] C.D. Eisenbach, R.W. Lenz, Makromol. Chem. 180 (1979) 429–440, and references therein.
[34] H. Bestian, Angew. Chem., Int. Ed. 7 (1968) 278–285, and references therein.
[35] J.H. Pawlow, A.D. Sadow, A. Sen, Organometallics 16 (1997) 5659–5663.
[36] J.H. Pawlow, A.D. Sadow, A. Sen, Organometallics 16 (1997) 1339–1342.
[37] S. Kacker, S.J. Kim, A. Sen, Angew. Chem., Int. Ed. 37 (1998) 1251–1253.
[38] R.D. Dghaym, K.J. Yaccato, B.A. Arndtsen, Organometallics 17 (1998) 4–6.
[39] D. Lafrance, J.L. Davis, R. Dhawan, B.A. Arndtsen, Organometallics 20 (2001) 1128–1136.

[40] M. Allmendinger, M. Zintl, R. Eberhardt, G. Luinstra, F. Molnar, B. Rieger, J. Organomet Chem. 689 (2004) 971–979.
[41] M. Allmendinger, R. Eberhardt, G. Luinstra, B. Rieger, Macromol. Chem. Phys. 204 (2003) 564–569.
[42] M. Allmendinger, R. Eberhardt, G. Luinstra, B. Rieger, J. Am. Chem. Soc. 124 (2002) 5646–5647.
[43] T.L. Lee, H. Alper, Macromolecules 37 (2004) 2417–2421.
[44] D. Takeuchi, Y. Sakaguchi, K. Osakada, J. Polym. Sci., Part A 40 (2002) 4530–4537.
[45] K. Nakano, K. Fumitaka, K. Nozaki, J. Polym. Sci., Part A 42 (2004) 4666–4670.
[46] L. Jia, E. Ding, W.R. Anderson, Chem. Commun. (2001) 1436–1437.
[47] L. Jia, H. Sun, J.T. Shay, A.M. Allgeier, S.D. Hanton, J. Am. Chem. Soc. 124 (2002) 7282–7283.
[48] J. Zhao, E. Ding, L. Jia, J. Polym. Sci., Part A 41 (2003) 376–385, 7283.
[49] G. Liu, L. Jia, J. Am. Chem. Soc. 126 (2004) 14716–14717.
[50] H. Xu, J.A. Gladding, L. Jia, Inorg. Chim. Acta 357 (2004) 4024–4028.
[51] H. Xu, L. Jia, Org. Lett. 5 (2003) 1575–1577.
[52] G. Liu, L. Jia, unpublished results.
[53] D.J. Darensbourg, A.L. Phelps, N. Le Gall, L. Jia, J. Am. Chem. Soc. 126 (2004) 13808–13815.
[54] W.F. Edgell, J. Lyford, Inorg. Chem. 9 (1970) 1932–1933.
[55] W.A. Reeves, G.L. Drake Jr., C.L. Hoffpauir, J. Am. Chem. Soc. 73 (1951) 3522–3523.
[56] R.F. Heck, D.S. Breslow, J. Am. Chem. Soc. 739 (1951) 3522–3523.
[57] R. Blessing, Acta Cryst. A 51 (1995) 33–38.
[58] SAINT+ V6.45, Bruker Analytical X-ray Systems, Madison, WI, 2003.
[59] SHELXTL V6.14, Bruker Analytical X-ray Systems, Madison, WI, 2000.
[60] M.C. Burla, M. Camalli, B. Carrozzini, G.L. Cascarano, C. Giacovazzo, G. Polidori, R. Spagna, J. Appl. Cryst. 36 (2003) 1103.
[61] C.A. Tolman, Chem. Rev. 77 (1977) 313–348.
[62] R.W. Johnson, R.G. Pearson, Inorg. Chem. 10 (1971) 2091–2095.